AD_____

Award Number: W81XWH-09-1-0405

TITLE: Understanding Collagen Organization in Breast Tumors to Predict and Prevent Metastasis

PRINCIPAL INVESTIGATOR:Edward Brown

CONTRACTING ORGANIZATION: University of Rochester
Rochester, NY 14642

REPORT DATE: September 2012

TYPE OF REPORT: Annual

PREPARED FOR: U.S. Army Medical Research and Materiel Command
Fort Detrick, Maryland 21702-5012

DISTRIBUTION STATEMENT:

√ Approved for public release; distribution unlimited

REPORT DOCUMENTATION PAGE

Form Approved
OMB No. 0704-0188

1. REPORT DATE	2. REPORT TYPE	3. DATES COVERED
09-1-2012	Annual	9-1-11 to 8-31-12

4. TITLE AND SUBTITLE
Understanding Collagen Organization in Breast Tumors to Predict and Prevent Metastasis

5a. CONTRACT NUMBER

5b. GRANT NUMBER
W81XWH-09-1-0405

5c. PROGRAM ELEMENT NUMBER

6. AUTHOR(S)
Edward Brown

edward_brown@urmc.rochester.edu

5d. PROJECT NUMBER

5e. TASK NUMBER

5f. WORK UNIT NUMBER

7. PERFORMING ORGANIZATION NAME(S) AND ADDRESS(ES)

University of Rochester
Rochester, NY 14642

8. PERFORMING ORGANIZATION REPORT NUMBER

9. SPONSORING / MONITORING AGENCY NAME(S) AND ADDRESS(ES)
U.S. Army Medical Research and Materiel Command
Fort Detrick, MD 21702-5012

10. SPONSOR/MONITOR'S ACRONYM(S)

11. SPONSOR/MONITOR'S REPORT NUMBER(S)

12. DISTRIBUTION / AVAILABILITY STATEMENT
Approved for public release; distribution unlimited

13. SUPPLEMENTARY NOTES

14. ABSTRACT
The ordering of collagen fibers within a tumor has significant influence on tumor metastasis: in murine breast tumor models, tumor cells move towards blood vessels along fibers that are visible via second harmonic generation (SHG), and SHG is exquisitely sensitive to molecular ordering. Tumor cells that are moving along SHG-producing (i.e. ordered) collagen fibers move significantly faster than those cells that are moving independently of SHG-producing fibers, and the extent of SHG-associated tumor cell motility is correlated with metastatic ability of the tumor model. Furthermore, the tumor-host interface of murine breast tumor models is characterized by radially oriented SHG-producing fibers associated with tumor cells invading the surrounding tissue. Consequently we believe that the process of establishing ordered fibers offers an exciting, and currently unexploited, therapeutic target. To take advantage of this, we must first learn the cellular players and molecular signals by which collagen ordering is induced. Therefore, in this application we propose to determine the key cells and signals which influence the ordering of collagen in breast tumors, determine if this ordering is predictive of metastasis, and develop new optical tools to study this ordering.

15. SUBJECT TERMS
Microscopy, metastasis

16. SECURITY CLASSIFICATION OF:			17. LIMITATION OF ABSTRACT	18. NUMBER OF PAGES	19a. NAME OF RESPONSIBLE PERSON
a. REPORT	b. ABSTRACT	c. THIS PAGE			Edward Brown, Ph.D.
U	U	U	UU	42	19b. TELEPHONE NUMBER *(include area code)* (585) 273-5918

Standard Form 298 (Rev. 8-98)
Prescribed by ANSI Std. Z39.18

Table of Contents

Introduction.

The extent and nature of the ordering of collagen fibers within a tumor has significant influence on the process of tumor metastasis: in murine breast tumor models, tumor cells move towards blood vessels along fibers that are visible via second harmonic generation (SHG), and SHG is exquisitely sensitive to molecular ordering (see below). Tumor cells that are moving along SHG-producing (i.e. ordered) collagen fibers move significantly faster than those cells that are moving independently of SHG-producing fibers, and the extent of SHG-associated tumor cell motility is correlated with metastatic ability of the tumor model. Furthermore, the tumor-host interface of murine breast tumor models is characterized by radially oriented SHG-producing fibers associated with tumor cells invading the surrounding tissue. Lastly, we have shown that treatment of tumors with the hormone relaxin, known to alter metastatic ability, alters the collagen ordering as detectable by SHG.

As locomotion along ordered (SHG-producing) fibers plays a pivotal role in the metastatic process, we believe that the process of establishing ordered fibers offers an exciting, and currently unexploited, therapeutic target. To take advantage of this, we must first learn the cellular players and molecular signals by which collagen ordering is induced. Therefore, in this application we propose to *determine the key cells and signals which influence the ordering of collagen in breast tumors*. We will do this by disrupting candidate cells and signals in mouse models of breast cancer using SHG-based measures of collagen ordering, and metastasis, as readouts. Additionally, we will *determine if SHG measures of collagen ordering in breast tumors are clinically useful predictors of metastatic outcome in breast cancer patient biopsies*.

This work will have great impact for several reasons. It will provide important insight into the molecular and cellular mechanisms by which the collagen in breast tumors is ordered, and how this ordering affects metastatic ability. In future work we can then exploit these findings by developing and evaluating clinically useful therapeutic techniques that will target, for the first time, the ordering of tumor collagen and hence attempt to inhibit metastatic ability, improving patient survival. This project will also explore whether collagen ordering in the tumor, as quantified by SHG, is a clinically viable predictor of metastatic outcome in patient biopsies. A measure of metastatic ability is extremely exciting, because there is currently an identified, pressing need for patient stratification based upon metastatic risk, in order to minimize 'over treatment' of patients who only require local therapy after resection, not systemic chemotherapy[6]. This would improve patients' quality of life. Hence, this project has promise to be clinically relevant through two separate paths.

Body

The Statement of Work for this grant proposal was as follows:

Statement of Work

Specific Aim 1. Determine the role of macrophages in governing collagen ordering in tumors, and their mechanism of action. (Months 1-30)

1a) Modulate the presence of macrophages, then evaluate the effects on collagen ordering in tumors, and the effects on metastatic burden. (Months 1-12) Uses liposome treatment. ~50 mice. Verifies involvement of macrophages' in collagen ordering in tumors, the exact nature of their particular impact on collagen ordering, and the impact on metastasis.

1b) Manipulate the expression of candidate genes in macrophages, and evaluate the effects on collagen ordering in tumors, and the effects on metastatic burden (Months 13-30) Uses bone marrow transfer after irradiation. Source animals are one of 7 knockouts, for 7 candidate genes. ~50x7= 350 mice. Produces identity of key signaling molecules involved in collagen ordering in tumors, the exact nature of their particular impact on collagen ordering, and the impact on metastasis.

Specific Aim 2. Determine the role of Th1, Th2, and Tregs in governing collagen ordering in tumors, and their mechanism of action. (Months 31-60)

2a) Modulate the presence of each cell type, then evaluate the effects on collagen ordering in tumors, and the effects on metastatic burden.(Months 31-42) Uses cell transfer after antibody treatment. ~3x50=150 mice. Produces identity of key cells involved in collagen ordering in tumors, the exact nature of their particular impact on collagen ordering, and the impact on metastasis.

2b) Manipulate the expression of candidate genes in those cell types found significant in 2a, and evaluate the effects on collagen ordering in tumors, and the effects on metastatic burden (Months 43-60) Uses cell transfer after antibody treatment. Source animals are one of 7 knockouts, for 7 candidate genes. ~3x50x7=1050 mice. Produces identity of key signaling molecules involved in collagen ordering in tumors, the exact nature of their particular impact on collagen ordering, and the impact on metastasis.

Specific Aim 3. Determine if collagen ordering is a clinically useful predictor of metastatic ability in human tissue samples (Months 1-60).

1a) In archival specimens from breast tumors we will evaluate the predictive relationships between collagen ordering and metastatic outcome (Months 1-60). Uses pathology samples of 4 breast tumor types to determine if SHG can predict metastatic outcome. ~4x50=200 samples. Produces an assessment of SHG's predictive ability.

Over the *previous* two years, as discussed in our previous yearly report, we demonstrated that in the E0771 breast tumor model, manipulation of tumor associated macrophages (TAMs) alters the ratio of SHG to collagen I antibody staining, as does manipulation of stromal TNF-a, and that the two effects were not additive. That suggests that either TAMs induce collagen manipulation through expression of TNF-a, or that stromal TNF-a induces collagen manipulation through its action on TAMs. In *this* yearly report I describe a series of follow-up experiments wherein we manipulate stromal expression of IL-10, as well as IFN-g, and observe the effects on SHG/staining ratios as well as metastatic outcome. This provides evidence implicating stromal TNF-a action on TAMs, and not TAM expression of TNF-a, as a key pathway regulating tumor matrix structure. In addition it provides evidence for an independent stromal pathway that affects matrix microstructure, presumably host T cells.

The remaining part of the report focuses on a series of experiments directly addressing the goals in Aim 3 of the statement of work, where we report on SHG studies of human breast tumor tissue microarrays, and reveal several interesting findings with those samples. As we have just summarized those results in a manuscript (in revision, Journal of Biomedical Optics), I will simply reproduce that manuscript as the final text of the yearly report.

Impact of Stromal IL-10 on collagen microstructure and metastasis.

E0771 produces IL-10, as do E0771-derived TAMs

Pilot experiments were conducted to determine if E0771 cells produce IL-10. E0771 cells cultured with 10% FCS to 75% confluence produce measurable IL-10 (Figure 1). By comparison, RAW264.7 macrophages were also tested at 75% confluence, produced measurable IL-10 in normal media and produced significantly elevated levels of IL-10 when activated with IL-4, a quintessential M2 polarization stimulus (Figure 1). To confirm that TAMs from E0771 tumors can produce IL-10, macrophages were isolated from E0771 tumors using magnetic antibody separation targeted to CD11b. These TAMs also produced IL-10 at detectable levels in culture, with or without activation by IL-4 (Figure 1). Furthermore, E0771 tumors were grown in both wildtype and IL-10(-/-) animals. IL-10 was readily detectable in wildtype-derived E0771 tumor lysates, as well as those grown in IL-10 (-/-) mice, indicating production of IL-10 by E0771 cells continues in vivo (Figure 2). Taken together, these results suggest that the E0771 cell line is a source of IL-10 production in vitro and in vivo, and that E0771-associated macrophages, as expected, are also a primary source of this signal in vivo.

Figure 1: IL-10 production by tumor cells and macrophages in vitro.

IL-10 is produced by E0771 breast tumor cells at detectable levels in vitro (leftmost bar, n=5 all groups). Macrophage-like RAW264.7 cells produce some IL-10 without stimulation, and significantly increase this production upon exposure to IL-4 at 50 ng/mL for 24 hours. IL-4 influences macrophages toward the M2 phenotype (alternative activation) and is considered characteristic of an immunosuppressive, anti-inflammatory environment. E0771-derived CD11b+ macrophages also produce a significant baseline quantity of IL-10, which interestingly cannot be subsequently elevated following IL-4 exposure (fourth and fifth bars respectively). These experiments indicate that IL-10 is produced in significant quantities by E0771-derived TAMs, as well as by E0771 tumor cells themselves. This leads to difficulties in interpreting results in IL-10-deficient mice, as discussed in the text.

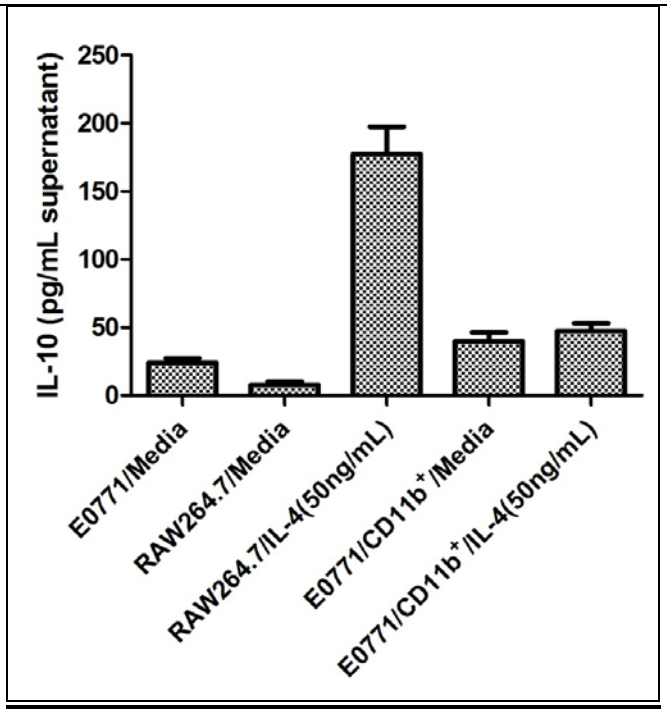

Figure 2: IL-10 is present in E0771 tumors in both wildtype mice and those lacking IL-10 expression.

In keeping with the results depicted in Figure 19, E0771 tumor lysates from tumors grown in wildtype mice show significant levels of IL-10 (left bar, n=5 both groups). The contribution of the E0771 tumor cells to IL-10 levels in the tumor is seen in the right bar, in which tumors are grown in IL-10-deficient mice. The difference between the two represents the stromal cell contribution to IL-10 production in the E0771 tumor. This difference is statistically significant ($p<0.05$).

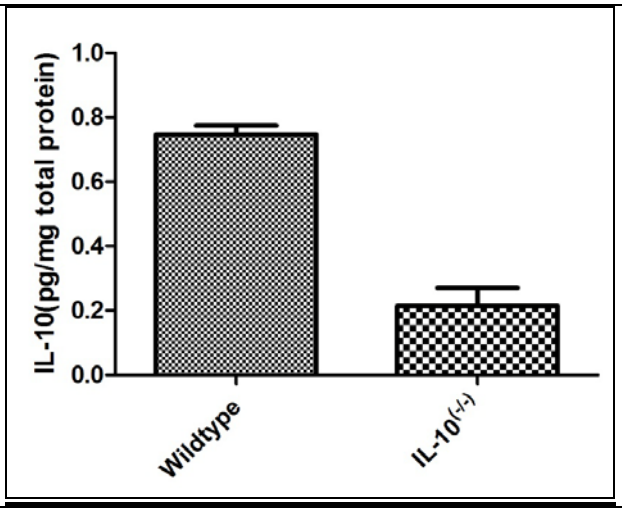

Effects of TAM depletion and IL-10 knockout on intensity of SHG-producing fibers

To determine if TAM depletion or stromal IL-10 knockout affects the intensity of SHG-producing fibers in the E0771 tumor, tumors were grown orthotopically in either wildtype or IL-10(-/-) mice treated with liposomes containing clodronate to deplete TAMs. Control mice were treated with liposomes containing PBS. Figure 3 shows the results of the experiment: by two-way ANOVA, a strong main effect of TAM depletion ($p<.0001$) was revealed, but no main effect of IL-10 knockout was observed ($p=.155$). Furthermore, the variables did not significantly interact ($p=.156$). In other words, TAM depletion reduces the intensity of SHG-producing fibers in E0771 tumors as before, and IL-10 knockout does not have a statistically significant effect upon intensity of SHG-producing fibers, in the presence or absence of TAMs.

Effects of TAM depletion and IL-10 knockout on fiber IF intensity

SHG is dependent upon collagen content as well as fiber microstructure. Therefore, in order to produce a measure of fiber microstructure, we must normalize the SHG intensity to the total amount of collagen I present. Consequently, we quantify collagen content using anti-collagen type I antibodies to detect collagen I IF. TAM depletion is again able to increase IF intensity in the E0771 breast tumor, but stromal IL-10 knockout does not alter detected collagen I fiber IF in the E0771 tumor (Figure 4). By two-way ANOVA, we see a strong main effect of TAM depletion but not IL-10 knockout ($p<.0001$, $p=.617$ respectively). Furthermore, the variables did not interact ($p=.249$). We therefore conclude that tumor growth in the presence of TAM depletion results in a significant increase in anti-collagen type I IF in E0771 tumors, but that growth in the absence of IL-10 has no effect on IF intensity.

Figure 3: Evaluation of alterations in collagen as visualized by SHG in the ECM of the E0771 breast tumor in response to perturbations in TAM presence and stromal IL-10 expression.

TAM depletion results in a significant and uniform decrease in collagen fiber SHG intensity regardless of IL-10 expression, whereas IL-10 deficiency is not sufficient to create a statistically significant difference in SHG fiber intensity. n = 21, 16, 9, and 8 respectively. Main Effect, TAM $p<.0001$, Main Effect, IL10 $p=0.1550$, Interaction, $p=0.1559$.

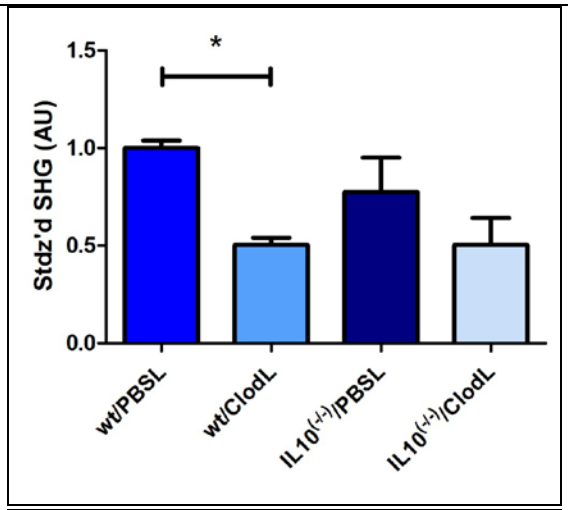

Figure 4: Evaluation of alterations in collagen as visualized by IF in the ECM of the E0771 breast tumor in response to perturbations in TAM presence and IL-10 expression.

TAM depletion, but not IL-10 knockout, is sufficient to alter IF intensity in the E0771 tumor. n=21, 16, 9, and 8 respectively. Main Effect, TAM $p<.0001$, Main Effect, IL10 $p<0.6168$, Interaction $p<0.2492$.

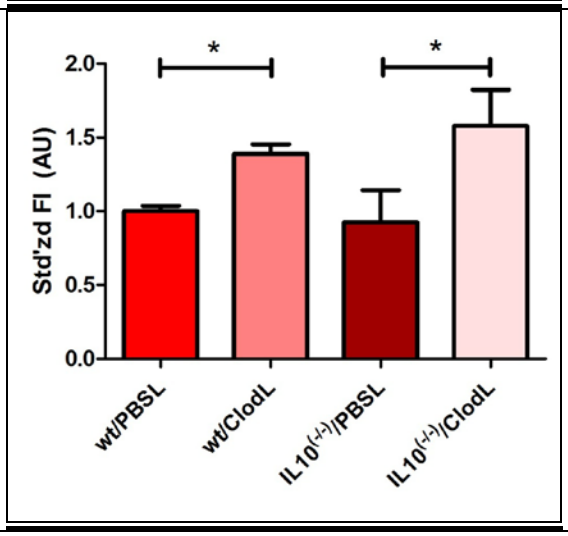

Effects of TAM depletion and IL-10 knockout on OI

Division of the SHG signal by the IF signal produces the order index (OI), which is primarily sensitive to changes in fiber microstructure, such as fibril diameter, spacing, and order versus disorder in fibrillar packing . Figure 5 shows that OI was significantly reduced by TAM depletion with ClodL, but not stromal knockout of IL-10, with a main effect of p<.0001 and p = .066 respectively, with no significant interaction (p=.635). This suggests that TAMs again influence OI, but stromal IL-10 in the presence or absence of TAMs does not.

Metastatic burden correlates with TAM presence, but not with IL-10 knockout

To ascertain a possible relationship between modulations in OI and modulations in metastatic burden, lungs were resected, sectioned, and stained with hematoxylin and eosin, then imaged to determine the extent of metastasis. Figure 6 depicts the incidence of lung metastasis in these animals. Two-way analysis of variance shows a strong main effect of TAM depletion, but not abrogation of IL-10, on metastatic burden (p=.002 and p= .333 respectively). The degree of interaction is insignificant (p=.113). We conclude that TAM depletion but not IL-10 knockout result in significant decreases in metastatic events, and that the decrease due to TAM depletion again correlates with changes in OI values in the E0771 tumor.

Figure 5: Evaluation of alterations in the SHG of the ECM in the breast tumor relative to total collagen I deposition (OI) in response to perturbations in TAM presence and IL-10 expression.

These data indicate that TAM depletion is capable of strongly regulating OI in the E0771 tumor, but that IL-10 deficiency is not sufficient to cause a change in OI. n=21, 16, 9 and 8. Main Effect, TAM p<.0001, Main Effect, IL10 p<0.0661. Interaction, p=0.6352.

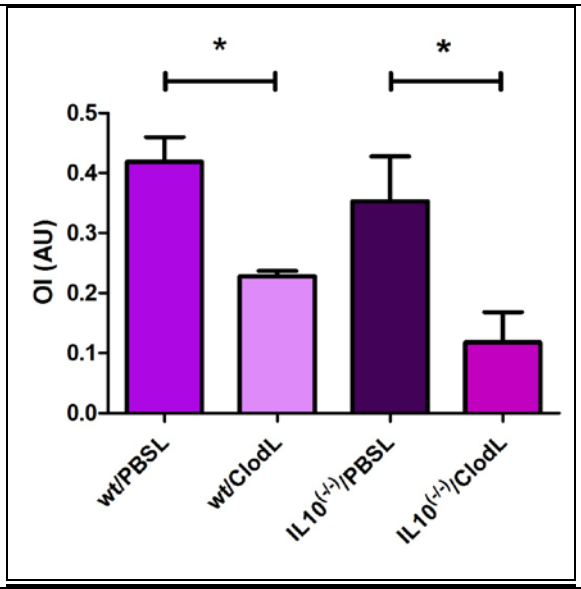

Figure 24: Evaluation of E0771 metastatic burden in the lung in response to perturbations in TAM presence and IL-10 expression.

Stromal IL-10 deficiency is not sufficient to decrease metastatic burden in the lung of the E0771-bearing mouse, but TAM depletion does produce a strongly uniform decrease in the amount of metastases present in 10 sections at 21 days. n = 21, 16, 9, and 8. Main Effect, TAM p=0.0024, Main Effect, IL10, p<0.3328, Interaction p=0.1134.

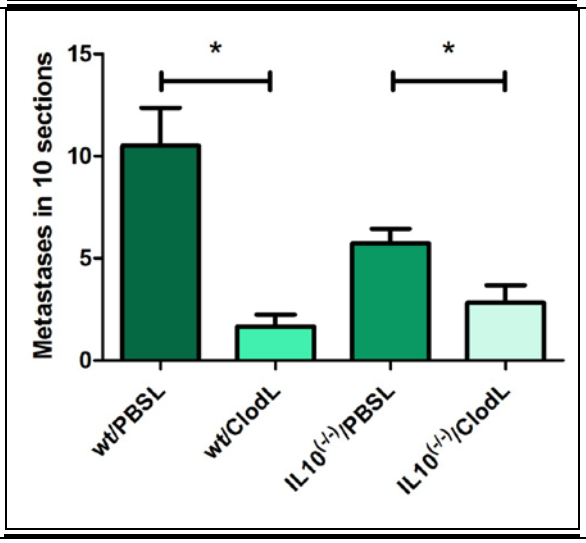

Discussion

We investigated whether manipulation of TAM populations and/or stromal IL-10 is able to alter the microstructure of collagen I fibers (as measured by the OI) and metastatic burden. Our OI data suggest that in the E0771 model of metastatic breast cancer, TAMs influence collagen microstructure, but that stromal IL-10 does not influence collagen microstructure. This inability of stromal IL-10 to affect OI is particularly interesting given IL-10's known role as a particularly potent inhibitor of macrophage production of TNF-a. Based upon the results in last year's yearly report we previously produced two likely models for the mechanism of TAM and stromal TNF-a's impact on collagen OI: Either 1) stromal TNF-a induces TAMs (and only TAMs) to alter collagen OI, or 2) TAMs express TNF-a (and only TNF-a) to alter collagen OI. The fact that significant modulation of IL-10 has no effect on the OI, and that IL-10 is an inhibitor of TAM production of TNF-a, suggests that Model 1 is more likely than Model 2.

There are three alternative possibilities, however. Figure 2 showed that by growing E0771 tumors in IL-10 KO mice we are only achieving a partial elimination of IL-10 in the tumor, due to IL-10 production by the tumor cells themselves. Therefore it is possible that we simply have not lowered IL-10 enough to see any effect of its modulation. An alternative possibility is that these mice, through a lifetime of being deprived of stromal IL-10, have compensated for its absence by up- or down- regulation of other signaling pathways. This compensation may have managed to reproduce the actions of IL-10 with other molecules, and hence any modulation induced in tumor OI is hidden. Finally, although it seems unlikely, it is possible that IL-10 does play a role in defining matrix microstructure, but that when we modulate IL-10 expression several changes in microstructure occur (for example a change in fibril spacing to increase SHG, combined with a change in fibril diameter to decrease SHG) such that their effects on OI exactly cancel out .

SHG reveals matrix alterations during breast cancer progression.

For this part of the yearly report, I will simply reproduce the recently written manuscript, currently in revision in Journal of Biomedical Optics. That follows on the next few pages.

SHG Reveals Matrix Alterations During Breast Tumor Progression

Kathleen Burke[1] and Edward Brown[1]

[1]Department of Biomedical Engineering, University of Rochester, Goergen Hall Box 270168, Rochester, NY, 14627, USA

Correspondence to:

Kathleen Burke
Department of Biomedical Engineering
University of Rochester
Goergen Hall Box 270168
Rochester, NY, 14627
Tel: 001-585-276-2254
Email: Kathleen_Burke@URMC.Rochester.edu

Edward Brown
Department of Biomedical Engineering
University of Rochester
Goergen Hall Box 270168
Rochester, NY, 14627
Tel: 001-585-273-5918
Email: Edward_Brown@URMC.Rochester.edu

Key words: Second Harmonic Generation, Forward to Backward Ratio, Breast cancer, Tumor Stage, Tumor Grade

Abstract

Alteration of the extracellular matrix in tumor stroma influences efficiency of cell locomotion away from the primary tumor into surrounding tissues and vasculature, thereby affecting metastatic potential. We studied matrix changes in breast cancer through the use of Second Harmonic Generation (SHG) of collagen in order to improve our current understanding of breast tumor stromal development as well as diagnostic capabilities of SHG. Specifically, we utilized a quantitative analysis of the ratio of forward to backward propagating SHG signal (F/B ratio) to monitor collagen structure throughout ductal and lobular carcinoma development. After detection of a significant decrease in the F/B ratio of Invasive but not *in situ* Ductal Carcinoma compared to healthy tissue, the collagen F/B ratio was investigated to determine the evolution of structural changes throughout tumor progression. Results were compared to the progression of Lobular Carcinoma, whose F/B signature also underwent significant evolution during progression, albeit in a different manner, which offers insight into varying methods of tissue penetration and collagen restructuring between the carcinomas. This research outlines trends of stromal reorganization throughout breast tumor development and has implications for potential applications of SHG used with pathological analysis as a biomarker of primary tumor growth and metastatic potential.

Introduction

There are two primary forms of invasive breast carcinomas, ductal and lobular, named after the breast structure from which they originate. The replication of tumor cells within these structures without interacting with the surrounding tissue is called Carcinoma *in Situ*, where Ductal Carcinoma *in situ* (DCIS) makes up 25-30% of all diagnosed breast cancer [1]. 75-80% of invasive breast carcinomas are categorized as Invasive Ductal Carcinoma (IDC) [2], which is the progression of a primary tumor from within the breast duct to an invasion of surrounding tissue by penetrating through the basement membrane of the duct. Invasive Lobular Carcinoma (ILC) is the invasive growth of cancer cells which originate in the lobules and penetrate the surrounding breast tissue. Lobular Carcinoma *in situ* (LCIS) is characterized not as cancer and not as a predecessor to ILC, but rather a benign growth of abnormal cells that are commonly undetectable by mammograms but if detected (usually in biopsies taken for other reasons) can serve as a marker for increased risk of future invasive carcinomas (ILC or IDC) in either breast [3]. With the increased capabilities of early detection and treatment of cancer, mortality rates due to the primary tumor have decreased, and currently 90% of cancer mortality is a result of metastatic events [4]. It is therefore becoming increasingly important to uncover prognostic markers that can predict the metastatic potential of a primary tumor to aid in determining the optimal course of patient treatment, as well as for assisting in the creation of new methods of treatment. Previous research points to tumor size [5, 6], lymph-node status [6], grade [7], urokinase plasminogen activator (uPA) protein levels [8, 9], as well as other genetic and physiological factors of the tumor to predict levels of metastasis [10]. Changes in these factors are accompanied by changes in the extracellular matrix (ECM) in the tumor stroma [10, 11, 12], that result from the release of signals and proteases from surrounding stromal cells such as

cancer associated fibroblasts [13] and macrophages [14]. A major focus of ECM modification is alterations in collagen, including degradation of collagen IV, XV, & XVIII in the basement membrane surrounding the tumor [15], and remodeling of collagen I throughout the connective tissue [13, 16, 17]. Modified fibrillar collagen in the connective tissue allows for a more efficient dispersal of tumor cells into the surrounding tissue and vasculature to spread to a secondary location [16, 17].

Second Harmonic Generation (SHG) is a scattering phenomenon, in which two incoming photons are scattered by a non-centrosymmetric structure into one photon of exactly half the wavelength. The resultant emission is coherent, hence the directionality, intensity, and polarization of the outgoing light is sensitive to various structural parameters of the scatterers including scatterer order and spacing, angle, as well as overall spatial extent of the scatterer distribution along the laser axis [18, 19, 20]. Collagen, primarily type I collagen, is capable of producing an SHG signal that can be detected in biological samples and used as a technique for monitoring the changes in ECM structure throughout tumor development. This technique results in high resolution two-photon images without the need for fluorescent staining and without photobleaching, and can applied to the surface of a primary tumor, excised tissue, or a sectioned sample to provide insight into matrix structure and aid in clinical diagnostics.

The progression of breast tumors is diagnosed along a two axis classification scheme, based upon the ability to visually differentiate the tumor cells from healthy cells, as well as the stage of the growth and metastatic properties of the tumor. Fenhalls *et al.* used northern analysis of tumor samples to show that tumor staging is accompanied by changes in the level of collagen mRNA

[21]. Following this study many groups have incorporated two-photon techniques to analyze collagen SHG signals in an attempt to differentiate healthy and tumor tissue. Morphological collagen changes, such as the shape of fibrillar collagen [22] or its orientation with regards to the border of the primary tumor [23], have been investigated in order to differentiate between healthy and malignant tumors as well as to predict survival rates associated with primary tumor samples. Further studies have incorporated third harmonic generation signals [24] or intrinsic fluorescence analysis [25, 26] to increase the morphological information provided by a tumor sample and to standardize quantitative SHG measurements using the ratio of SHG/two-photon excited fluorescence (TPEF). In a mouse model of epithelial carcinoma SHG and TPEF of intrinsic signals was used to track the progression of tumors throughout different pathological phases [27]. Zhuo *et al.* showed that backward propagating SHG of freshly removed ectocervical samples could be used to differentiate between healthy tissue, cervical intraepithelial neoplasia (precancer) and cancer, showing the potential of SHG techniques to not only differentiate between healthy and tumor tissue intra-operatively but to provide insight into the progression of the tumor [28].

The ratio of the forward to backward propagating SHG signal (F/B ratio) is sensitive to the spatial extent of the scatterers along the optical axis (in collagen, the effective fibril diameter) as well as order versus disorder in fibril packing [18, 19, 20]. In this study we will use the phrase "collagen structure" to indicate those properties of an individual collagen fiber which influence SHG F/B from that fiber, as distinct from "collagen morphology" which will indicate macroscopic properties such as fiber orientation, tortuosity, and overall density of fibers. It has been shown previously that the F/B ratio can be used to differentiate between healthy and tumor

ovarian cancer [29], which is particularly interesting because F/B analysis is intrinsically ratiometric and hence is less susceptible to variations in excitation intensity, and is also less susceptible to user-to-user variability of morphology-based analysis techniques. We are interested in exploring the application of F/B imaging to breast tumor samples both to learn about the evolution of fibrillar collagen structure during tumor progression as well as to explore the possibility of using this modality as a biomarker to assist in the classification of breast tumor samples *in vitro* or *in vivo*.

Methods

Breast Cancer Tissue Samples

The samples used throughout this study are primarily tissue microarray (TMA) slides, which are composed of 0.6-1.0mm diameter samples from cylindrical cores of paraffin embedded tissue specimens sectioned into 5μm thick slices. One advantage of these samples is that due to their thickness the effects of subsequent scattering or absorption of SHG light is negligible (μ_a~20 cm^{-1}, $\mu'_s \sim 10\ cm^{-1}$ [30, 31]). Each 5 μm thick, ~1.0 mm diameter specimen corresponds to a different patient/tumor and is mounted on a slide, with several tens of samples on each slide. The tumor specimens are staged by a certified pathologist, and every 10^{th} section of the TMA block is used to create an H&E stained slide which is analyzed by the pathologist to ensure that each sample is within the tumor and demonstrates properties of the diagnosis. Hence in the direction perpendicular to the plane of the sample, each tissue section is at least 50 microns from the tumor surface. In the plane of the sample, sections are chosen that are entirely within the tumor and do not contain significant healthy tissue, based upon inspection of the adjacent H&E stained slides. However, the distance from the outer edge of the core to the tumor surface is not known.

Consequently any significant variation of tumor SHG properties with distance from the tumor edge may increase the variance in our measurements.

The breast cancer tissue microarray samples that were used throughout this study came from two sources. Samples of healthy breast tissue, as well as various grades and stages of IDC and ILC, were purchased from Biomax (Rockville MD, slides BR1921, BR20830, BR805, BR961 and BR954). Pure DCIS and IDC tissue microarray slides were received from Dr. Ping Tang, and created in the Department of Pathology and Laboratory Medicine at the University of Rochester Medical Center.

In addition to the tissue microarray samples, several LCIS and ILC samples were generated from paraffin embedded tissue blocks (courtesy of Dr. Ping Tang), cut to 5 micron thickness. Table 1 summarizes which samples were used to create each data set.

Invasive breast tumors are graded on a 3-state classification system dependent upon tubule formation, nuclear polymorphism, and mitotic count, where Grade 1 has the most differentiated tissue with the best prognosis and Grade 3 is the least differentiated with the worst prognosis. The TNM staging system is a method of tumor classification determined by the size of the primary tumor (T), regional lymph node involvement (N) and presence of distant metastases (M). Staging of the primary tumor (T) as well as the metastatic events in the lymph node (N) incorporates multiple degrees of staging as opposed to metastatic staging (M), which is a binary system determined simply by the presence or absence of a distant metastases. The primary tumor staging is split into categories based on tumor diameters of between 1-20mm (T1), between 20-

50mm (T2), and greater than 50mm (T3). Tumors that have penetrated the chest wall or skin, independent of the size of the tumor are staged as T4 tumors. The lymph node (LN) staging scale begins at N0 indicating that there are no metastatic events present in the LN that are greater than 0.2mm or 200 cells. The two middle stages, N1 and N2, describe increasing involvement in the axillary LNs, or metastasis to the internal mammary LNs without spread to the axillary LNs. Specifically N1 tumors have either micrometastases, 1-3 axillary LN metastases, or sentinel LN metastases detected through biopsy. N2 tumors are characterized by 4-9 axillary LN metastases, or clinically detected sentinel LN metastases. N3 stage is the most far reaching metastatic LN events, including either greater than 10 axillary events with at least one event greater than 2mm, infraclavicular LN metastases, or clinically detected internal mammary and axillary LN metastases [32]. All samples were classified based upon the aforementioned grading and staging scheme by a certified pathologist and all parties were blinded to the classification of the samples during image acquisition and analysis.

Imaging

The excitation light is a Spectra Physics MaiTai Ti:Sapphire laser at 810nm, with 100fs pulses at 80MHz. It is directed to the sample through an Olympus BX61WI upright microscope, with beam scanning and image acquisition controlled by a n Olympus Fluoview FV300 scanning system. Before entering the scan box the laser passes through a Berek compensator (Model 5540, New Focus) adjusted such that the excitation light reaching the objective lens is circularly polarized (verified as <2% variation in transmitted power versus angle of an analyzer set after the dichroic and before the objective lens). An Olympus UMPLFL20XW water immersion lens (20×, 0.5 N.A.) is used to focus excitation light and capture backward propagating SHG signal.

After passing through the objective the signal is separated from the excitation beam using a 670nm short pass dichroic mirror, filtered using a 405nm filter (HQ405/30m-2P, Chroma, Rockingham, VT), and collected by a photomultiplier tube (Hamamatsu HC125-02). In the forward direction an Olympus 0.9 NA optical condenser was used to collect the signal, reflected by a 475nm long pass dichroic mirror (475 DCSX, Chroma, Rockingham, VT) in order to remove excess excitation light, filtered by a 405nm filter (HQ405/30m-2P, Chroma, Rockingham, VT) and captured by photomultiplier tube (Hamamatsu HC125-02).

Analysis

Forward and backward images were simultaneously collected as a stack of 11 images spaced 3μm apart, with a 660 μm field of view. One stack was made from the geometric center of each TMA sample. For the non-TMA samples, the image field in an unstained section was chosen based upon imaging of an adjacent H&E stained section to identify the center of the visible tumor structure. Image Analysis was conducted in with ImageJ Software [33]. Each stack was maximum intensity projected, serving as an "autofocus" for the effectively single layer of collagen that exists in these 5 micron sections and producing a single image pair for each sample. Projected images were background subtracted using a maximum intensity projection of an 11 image scan taken with a closed shutter. Day to day variations in optical alignments were accounted for by imaging one tissue sample (not included in the data pool) each day as a standard SHG sample and determining a normalization factor for each detector pathway that rendered the signal from that standard sample constant over time. For each image a common threshold was applied to all images taken in that imaging session and chosen by a blinded observer to distinguish collagen pixels from background pixels. The threshold of the backward

collected image was then used to create a mask, in which all of the pixels above threshold were set to 1, and all of the pixels below the threshold were zero. That mask was then used to exclude background (i.e. non-fiber) pixels from consideration and the average pixel value of fiber (i.e. non-background) pixels was calculated from an F/B ratio image. Due to the small sample thickness (5 μm) we assume that the measured F/B ratio is due solely to the original ratio of forward-emitted and backward-emitted SHG and is not significantly affected by s ubsequent backscattering of either component [30, 31].

Statistics

Statistical Analysis was performed using Prism 5 software (GraphPad, La Jolla, CA). Statistically significant data was defined as a p-value less than 0.05. Comparisons of two groups were analyzed using unpaired student t-tests. If the f-test for this data returned a value <0.05, a Mann-Whitney nonparametric t-test was used. For grouped analysis a one-way ANOVA was used with a Newman-Keuls Multiple Comparison post-hoc test to determine the difference between groups. If the Barrett's test for equal variance results in a p-value less than 0.05, a non-parametric Kruskal-Wallis test with a Dunn's post-hoc test was performed.

Results

Figure 1 s hows images of backscattered SHG signal and F/B ratio as compared to tissue structures apparent in H&E staining, taken from the same section of healthy and tumor samples. Note that while H&E staining has no significant effect on the SHG signal intensity ($p < 0.05$, data not shown), in this paper all quantitative F/B analysis was done on unstained slides. These example SHG images demonstrate some typical collagen morphological changes that occur

through the progression of ductal and lobular carcinoma, including changes in density, length, and organization of fibrillar collagen as seen in, for example, the "healthy" SHG image which has an appearance of many wavy fibers matted together, versus the "IDC" image where the collagen appears to form sparser, longer, and straighter fibers.

Changes in SHG F/B ratio were first analyzed in the progression from healthy tissue to DCIS to IDC, as shown in Figure 2a. The DCIS samples did not differ significantly from the healthy samples, but both the healthy and the DCIS samples had a significantly higher F/B ratio then the IDC samples. This led to the question of whether all IDC tumors are immediately differentiable from healthy tissue or if there is an evolution of the fibrillar collagen structure that becomes significantly different at a specific grade or stage. Looking first at tumor grade, which signifies how different the tumor cells appear in comaprison to healthy cells, it was apparent that Grade 1 tumors were not significantly different then healthy tissue (Figure 2b). As this tumor type progressed to Grade 2, it developed a significantly lower F/B ratio which remained at approximately this level for Grade 3 tumors as well.

Tumor staging is determined by the TMN system, which is dependent on 3 different properties of the tumor including its size (T), extent of LN metastatic events (N), and metastasis to sites other than LNs (M). The F/B ratio was measured as a function of these three categories to determine the change of collagen structure throughout different stages of tumor development. The F/B ratio was significantly lower in all stages of T-progression than in healthy tissue, but there were no differences or noticeable trends throughout the groups (Figure 3a).

One of the more interesting questions regarding the use of SHG analysis to study breast cancer progression is how the structure of fibrillar collagen in the primary tumor (as indicated by SHG F/B) relates to the potential of the tumor to metastasize. Figure 3b shows that the binary M-status did not have a significant effect on the F/B ratio. However this M-status is coarse, in that it divides tumors up into only two categories, those with and without known metastases to distant organs other than the lymph nodes. It is possible to further test the relationship between SHG F/B and metastatic potential of a tumor by looking at N-stage progression, which increases through four classification stages dependent upon the severity of LN involvement in metastatic events. This gives a more detailed description than M-status, because metastatic events in the LNs are more commonly detected than in other secondary sites, and the scale of progression is more finely detailed than the simple binary grading of the M-status. Figure 3c shows that between healthy tissue and tumors that are not metastatic to the LNs (N0) or minimally metastatic breast tumors (N1, N2) there is a significant decrease in the F/B ratio of SHG^{+} pixels relative to healthy tissue. However, in the N3 stage F/B is not different from healthy tissue. We then pooled the N0, N1, and N2 data and compared this pooled set to the N3 data. This allows us to compare SHG F/B for highly metastatic IDC tumors which have either greater than 10 axillary events with at least one event greater than 2 mm, infraclavicular LN metastases, or clinically detected internal mammary and axillary LN metastases (i.e. N3), versus those less metastatic IDC tumors which do not have any of those properties (i.e. N0, N1, or N2). This reveals a statistically significant difference between the two groups (Figure 3d).

In order to gain further understanding of breast cancer progression the same analysis was run on ILC samples, to understand how SHG F/B evolves after initiation of the tumor in a different

location. ILC showed a significant decrease in F/B ratio compared to healthy tissue, but was not significantly different from the ratio of IDC (Figure 4a). In contrast to the behavior of F/B in ductal carcinoma, Lobular Carcinoma *in situ* (LCIS) showed a significant decrease in F/B ratio relative to healthy breast, with no significant difference between LCIS and ILC (Figure 4b). The N-status analysis showed that there was a significant decrease in the F/B ratio for all N groups relative to healthy tissue, with no significant difference between any of the stages studied, similar to the trend of IDC for groups N0-N2 (Figure 4c) but unlike the behavior of IDC N3 tumors. Analysis of the effects of T-status on the fibrillar collagen showed that the F/B ratio decreased significantly between healthy tissue and T1, T2, and T3, stages while T4 is no longer differentiable from healthy tissue (Figure 4d). T4 is characterized by the interaction of *any* size tumors with either the chest wall or the skin, hence we pooled the other T stages of tumor (producing a group of any sized tumor that does not interact with the chest wall nor the skin) and compare the pooled group to the T4 tumors, demonstrating a significant difference in the F/B ratio (Figure 4e) between these two groups.

Discussion

We analyzed SHG F/B images throughout breast tumor progression in order to understand how this optical signature, which is influenced by fibrillar collagen structure, evolved alongside the tumor size, cell morphology, and metastatic changes that determine the grade and stage of the tumor. This provided several insights into the biology of ductal and lobular carcinoma, as well as insights into the possibility of using SHG F/B to assist in detection and/or diagnosis of breast cancer.

Biology of Ductal Carcinoma

The changes in collagen structure as indicated by SHG F/B in Figure 2a demonstrate that there is no significant alteration in fibrillar collagen structure between healthy breast tissue and ductal carcinoma *in situ*, but that there is an alteration in the structure of the collagen as the tumor progresses from an *in situ* to an invasive carcinoma. This is consistent with the fact that the majority of SHG^{+} collagen fibers in healthy tissue are surrounding the ducts, so as the tumor cells exclusively fill in the ducts in DCIS the surrounding collagen structure remains relatively unaffected. It is only when the tumor cells begin to invade the breast tissue outside of the duct that they induce changes in structure of the surrounding fibrillar collagen, as observed in the statistically significant difference between SHG F/B of IDC and healthy breast tissue (Figure 2a).

Taking a closer look at this phenomenon, we examined whether invasion through the basement membrane into the surrounding tissue (i.e. the transition from DCIS to IDC) causes an *immediate* change in the F/B ratio by comparing SHG F/B to the grade of the IDC tumor (Figure 2b). Our results showed that in Grade 1 IDC the F/B ratio is still *not* significantly different from the DCIS tissue nor the healthy tissue, but as IDC progresses to a Grade 2 or 3 tumor the SHG F/B ratio becomes significantly different. This suggests that the overall fibrillar collagen structure as determined by the F/B ratio is constantly evolving away from the healthy state as the IDC tumor cells become less differentiated.

Regarding the changes in primary tumor F/B seen throughout IDC tumor staging, there is interestingly no difference between the IDC samples that are at different primary tumor sizes (T stage), although they are all different than the healthy tissue cohort. Presumably, the transition

from healthy to tumor SHG F/B occurs when tumors are small enough to not be included in our cohorts of tumor samples, which means that it occurs when the tumor diameter is less than 1mm. Once tumors are greater than 1mm and hence large enough to be included in the T1-4 grading scheme, the size of the primary tumor does not influence collagen structure as quantified by SHG F/B. Combined with the fact that F/B of Grade 1 IDC does *not* differ significantly from healthy tissue, this suggests that during early tumor growth and progression there is a complex interplay between tumor size and grade, whereby small high grade tumors may produce a more significantly altered matrix than larger low grade ones.

As tumors progress from healthy to N0 (IDC with no LN involvement), the SHG F/B ratio statistically significantly decreases, and remains low as tumors progress to N1 (small metastatic events or $\leq$ 3 axillary events) and N2 (4-9 axillary events or clinically detected internal mammary LN metastases). Interestingly, as tumors progress to N3 stage (>10 axillary events, further reaching LN metastases, or metastases to both internal mammary and axillary LN) SHG F/B becomes indistinguishable from healthy F/B (Figure 3c) and is markedly different from the pooled group of other IDC tumors (Figure 3d). This evolution of SHG F/B suggests two intriguing possibilities. The first is based upon the view that N-stage progression is a chronological progression, with a single IDC advancing from having no LN metastases, through the subsequent N stages, and ending as an IDC with distant LN metastases. From that perspective, this data demonstrates that during tumor progression fibrillar collagen structure evolves in ways that affect SHG F/B, and raises the possibility that this evolution may influence efficient travel of metastatic tumor cells to distant LNs. After the initial evolution of collagen structure from normal to abnormal as the tissue progresses from healthy to an N0 tumor, there is

a subsequent "normalization" of collagen structure back to the structure of healthy fibrillar collagen (as quantified by F/B) that may facilitate distant metastasis and lead to the N3 highly metastatic case. Alternatively, these matrix changes may not represent an evolution of individual tumors in time, but suggest instead that those tumors that do NOT undergo an initial decrease in SHG F/B as the tissue first progresses from healthy to cancerous, and maintain a high F/B, may be more likely to produce extensive distant metastases. Although the F/B ratio reveals that there is a similarity in the collagen structure between the N3 tumor and healthy tissue, inspection of SHG images of healthy and N3 samples reveal that these similarities do not extend to the overall morphology of the fibers, as these are noticeably different between the two tissue states as shown in Figure 4d.

In traditional M staging, IDC tumors are divided up into M0 (no known metastases to distant non-lymph-node organs), and M1 (any number of metastases to distant non-lymph-node organs). For IDC tumors there is no relationship between SHG F/B and M status group (Figure 3b). This suggests either that there is no relationship between fibrillar collagen structure and the ability of the IDC to metastasize to different (non-LN) organs, or that the act of pooling all numbers of metastases to any non-LN organs into the single category of "M1" has hidden any subtle differences such as those that were evident in IDC when classified according to the more finely divided N stage classification scheme.

Biology of Lobular Carcinoma

Like IDC, ILC causes a change in the fibrillar collagen structure in breast tissue, as indicated by a decrease in the F/B ratio relative to healthy tissue (Figure 4a). However, LCIS F/B is

significantly different from healthy tissue F/B whereas DCIS is not (Figure 4b). This difference in matrix alterations is consistent with the significant difference in behavior of the two diseases. Unlike DCIS, which is categorized as cancer and if left untreated is likely to progress to IDC, [34] LCIS is described as a development of abnormal cells which is not believed to progress to ILC (although it does correlate with increased likelihood of the patient developing ILC or IDC later in life) [3].

In contrast to IDC, the stage of LN involvement (Figure 4c) has no effect on the F/B ratio of ILC, and all N stages are statistically different from healthy tissue. The stable F/B ratio throughout increasing LN involvement could result from the ILC's characteristic lack of a strong inflammatory response after penetrating the basement membrane [35], a response which would otherwise aid in the restructuring of the stromal collagen through recruitment of fibroblasts and macrophages [13, 14]. In ILC there is a change in SHG F/B with tumor T stage, specifically a loss of F/B difference relative to healthy tissue that occurs in the T4 stage of tumor progression (Figure 4c,d), which is when the tumor interacts with structures surrounding the breast tissue such as chest and skin. The marked difference between behavior of IDC and ILC at this stage contrasts with the close quantitative similarity of F/B values between the tumor types at earlier T stages (compare Figures 3a and 4d). This suggests that the mechanisms by which ILC and IDC recruit stromal cells to produce the collagenous matrix is subtly different, a difference that only becomes evident once the source of stromal cells shifts from breast tissue to the chest wall and/or the skin.

Detection and diagnosis

In addition to providing a window into the biology of the collagenous matrix of ductal and lobular carcinoma of the breast, these experiments also provide insights into the prospect of using SHG F/B as a biomarker to assist in detection and/or diagnosis of breast cancer, as has been explored in ovarian cancer [29]. In current breast conservation surgery, tumor tissue is removed and sent to pathology for subsequent analysis. If the circumference, or margin, of the excised tissue is found to contain tumor tissue within ~1 mm of the cut surface, there is a high risk that the adjacent edge of this tissue, still in the patient, also has tumor tissue. Consequently the patient must return to the hospital for a second and possible third surgery until surgical margins are found to be clear of tumor tissue. The multiple trips to the operating room and multiple surgeries seriously impact the patient's quality of life. Consequently, many groups are investigating optical techniques to provide more information to the surgeon, in the operating room, to rapidly assist in detecting the presence of tumor tissue near the resected margins and hence improve the odds that samples will be found to have tumor-free margins upon subsequent pathological analysis [36, 37, 38, 39]. The first step in evaluating the potential of the SHG F/B ratio to contribute to tumor assessment is to determine whether there is a detectable difference between healthy and tumor tissue, and to what degree this differentiation exists among tumors of different stage and grade. We find that LCIS, IDC and ILC, but not DCIS, can produce statistically significant differences in SHG F/B in the surrounding matrix. Furthermore, even the smallest tumors studied, T1 tumors, had a statistically significant SHG F/B from healthy tissue in both IDC and ILC. This, combined with recent demonstration of a method to quantify SHG F/B with a single objective lens [40] allows the possibility of using SHG F/B, perhaps along with other optical signatures, to assist in the real-time evaluation of tumor tissue during IDC and ILC

breast conserving surgery (LCIS is generally not treated surgically). The future clinical utility of SHG F/B will rely on the geometry of cut surfaces required to access the tissue for such an application, and the on further development of the single objective lens technique [40], or other techniques [29], as methods that can detect the F/B ratio from an intact [40] or coarsely sectioned [29] piece of tissue.

Conversely, the prognosis of using SHG F/B to detect tumor margins appears to be *negatively* impacted by the fact that SHG F/B evolves with IDC tumor grade, and specifically that Grade 1 IDC is hence indistinguishable from healthy tissue. Furthermore, F/B of the most metastatic form of IDC (N3) is not different from healthy tissue, nor is the largest (T4) form of ILC. Therefore, the ability of SHG F/B to provide a useful biomarker relevant to tumor detection/margin analysis would therefore be dependent upon the type, stage, and grade of tumor.

After tumor resection patients are frequently subjected to chemotherapy and radiation in an attempt to eliminate metastases, and an estimated 70% of patients are believed to be "overtreated" and receive chemotherapy/radiation in spite of not actually having distant metastases [10]. Consequently methods to predict metastatic outcome and reduce "overtreatment" are highly desirable in order to improve quality of life [10]. The results presented here demonstrate that in IDC, but not ILC, the SHG F/B ratio scales with the presence of distant LN metastases, although it does not scale with the presence of metastases to distant organs. This suggests that F/B may provide useful, albeit limited, information as to the metastatic output of IDC tumors and hence may assist in treatment planning.

Conclusion

This study has shown a series of collagen structural changes, as evaluated with SHG F/B, that occur throughout ductal and lobular carcinoma progression, including those that accompany growth, metastasis and changes in tissue morphology. SHG F/B has revealed a surprisingly complex evolution of matrix structure with grade and T, N, and M stage with perhaps the most interesting result being the fact that IDC tumors with the most "normal" F/B values have the largest number of distant LN metastases. This offers the possibility that either developing breast tumors undergo a "normalization" of collagen structure (but not macroscopic morphology) that correlates with enhanced distant metastases, or that those tissues that retain their healthy collagen structure upon transition to IDC are most likely to produce significant numbers of distant metastases. In addition to insights into the basic biology of the breast tumor extracellular matrix, these results suggest that in the future SHG F/B may be used in conjunction with pathological analysis to provide an additional biomarker about the metastatic potential of the IDC primary tumor, and to assist in margin detection in high-grade IDC as well as ILC tumors.

Acknowledgements and Funding

This work was funded by Department of Defense Breast Cancer Research Program (BCRP) Era of Hope Scholar Research Award W81XWH-09-1-0405 and NIH Director's New Innovator Award 1DP2OD006501). The authors would like to thank Dr. Ping Tang for generously supplying samples, as well as Drs. Seth Perry, Kelley Madden, and Ania Majewska for helpful discussions.

References

1. S Bianchi and V Vezzosi. "Microinvasive carcinoma of the breast." *Pathology and Oncology Research*. **14**(2):105-11 (2008).
2. GD Leonard and SM Swain. "Ductal carcinoma in situ, complexities and challenges." *Journal of the National Cancer Institute* **96**(12):906-20 (2004).
3. RV Hutter, RE Snyder, JC Lucas, FW Foote Jr, and JH Farrow. "Clinical and pathologic correlation with mammographic findings in lobular carcinoma in situ." *Cancer*. **23**(4):826-39 (1969).
4. ER Fisher, RM Gregorio, B Fisher, C Redmond, F Vellios, and SC Sommers. "The pathology of invasive breast cancer. A syllabus derived from findings of the National Surgical Adjuvant Breast Project (protocol no. 4)." *Cancer* **36**(1):1-85 (1975).
5. S Koscielny, M Tubiana, MG Lê, AJ Valleron, H Mouriesse, G Contesso, and D Sarrazin. "Breast cancer: relationship between the size of the primary tumour and the probability of metastatic dissemination." *British Journal of Cancer* **49**(6):709-15 (1984).
6. CL Carter, C Allen, and DE Henson. "Relation of tumor size, lymph node status, and survival in 24,740 breast cancer cases." *Cancer* **63**(1):181-7 (1989).
7. CW Elston and IO Ellis. Pathological prognostic factors in breast cancer. I. The value of histological grade in breast cancer: experience from a l arge study with long-term follow-up. *Histopathology* **41**(3A):154-61 (2002).
8. MP Look, WL van Putten, MJ Duffy, N Harbeck, IJ Christensen, C Thomssen, R Kates, F Spyratos, M Fernö, S Eppenberger-Castori, CG Sweep, K Ulm, JP Peyrat, PM Martin, H Magdelenat, N Brünner, C Duggan, BW Lisboa, PO Bendahl, V Quillien,

A Daver, G Ricolleau, ME Meijer-van Gelder, P Manders, WE Fiets, MA Blankenstein, P Broët, S Romain, G Daxenbichler, G Windbichler, T Cufer, S Borstnar, W Kueng, LV Beex, JG Klijn, N O'Higgins, U Eppenberger, F Jänicke, M Schmitt, and JA Foekens. "Pooled analysis of prognostic impact of urokinase-type plasminogen activator and its inhibitor PAI-1 in 8377 breast cancer patients." *Journal of the National Cancer Institute* **94**(2):116-28 (2002).

9. JA Foekens, HA Peters, MP Look, H Portengen, M Schmitt, MD Kramer, N Brünner, F Jänicke, ME Meijer-van Gelder, SC Henzen-Logmans, WL van Putten, and JG Klijn. "The urokinase system of plasminogen activation and prognosis in 2780 breast cancer patients." *Cancer Research* **60**(3):636-43 (2000).
10. B Weigelt, JL Peterse and LJ van't Veer. "Breast cancer metastasis: markers and models." *Nature Reviews Cancer* **5**: 591-602 (2005).
11. M Sund and R Kalluri. "Tumor stroma derived biomarkers in cancer." *Cancer Metastasis Reviews* **28**(1-2):177-83 (2009).
12. GP Gupta and J Massagué. "Cancer metastasis: building a framework.' *Cell.* **127**(4):679-95 (2006).
13. R Kalluri and M Zeisberg. "Fibroblasts in cancer." *Nature Reviews Cancer* **6**, 392-401 (2006).
14. JW Pollard. "Macrophages define the invasive microenvironment in breast cancer." *Journal of Leukocyte Biology* **84**(3):623-30 (2008).
15. R Kalluri. "Angiogenesis: Basement membranes: structure, assembly and role in tumour angiogenesis." *Nature Reviews Cancer* **3**, 422-433 (2003).

16. PP Provenzano, KW Eliceiri, JM Campbell, DR Inman, JG White, and PJ Keely. "Collagen reorganization at the tumor-stromal interface facilitates local invasion." *BMC Medicine* **4**(1), 38 (2006).

17. J Condeelis and JE Segall. "Intravital imaging of cell movement in tumours." *Nature Reviews Cancer* **3**(12): 921-30 (2003).

18. R Lacomb, O Nadiarnykh, SS Townsend, and PJ Campagnola. "Phase Matching considerations in Second Harmonic Generation from tissues: Effects on emission directionality, conversion efficiency and observed morphology." *Optics Communications* **281**(7):1823-1832 (2008).

19. J Mertz and L Moreaux. "Second-harmonic generation by f ocused excitation of inhomogeneously distributed scatterers." *Optics Communications* **196**(1–6): 325–330 (2001).

20. X Han, RM Burke, ML Zettel, P Tang and EB Brown. "Second harmonic properties of tumor collagen: determining the structural relationship between reactive stroma and healthy stroma." *Optics Express* **16**(3): 1846-1859 (2008).

21. G Fenhalls, M Geyp, DM Dent, and MI Parker. "Breast tumour cell-induced down-regulation of type I collagen mRNA in fibroblasts." *British Journal of Cancer* **81**(7): 1142–1149 (1999).

22. G Falzon, S Pearson and R Murison. "Analysis of collagen fibre shape changes in breast cancer." *Physics in Medicine and Biology* **53**, 6641 (2008).

23. MW Conklin, JC Eickhoff, KM Riching, CA Pehlke, KW Eliceiri, PP Provenzano, A Friedl and PJ Keely. "Aligned collagen is a prognostic signature for survival in human breast carcinoma." *American Journal of Pathology*. **178**(3), 1221-32 (2011).

24. SP Tai, TH Tsai, WJ Lee, DB Shieh, YH Liao, HY Huang, K Zhang, HL Liu and CK Sun. “Optical biopsy of fixed human skin with backward-collected optical harmonics signals.” *Optics Express* **13**(20), 8231-42 (2005).

25. RM Williams, A Flesken-Nikitin, LH Ellenson, DC Connolly, TC Hamilton, AY Nikitin and WR Zipfel. “Strategies for High-Resolution Imaging of Epithelial Ovarian Cancer by Laparoscopic Nonlinear Microscopy.” *Translational Oncology* **3**(3): 181–194 (2010).

26. ND Kirkpatrick, MA Brewer and U Utzinger. “Endogenous optical biomarkers of ovarian cancer evaluated with multiphoton microscopy.” *Cancer Epidemiology, Biomarkers and Prevention* **16**(10): 2048-57 (2007).

27. W Zheng, D Li, S Li, Y Zeng, Y Yang and JY Qu. “Diagnostic value of nonlinear optical signals from collagen matrix in the detection of epithelial precancer.” *Optics Letters* **36**(18):3620-2 (2011).

28. S Zhuo, J Chen, G Wu, S Xie, L Zheng, X Jiang and X Zhu “Quantitatively linking collagen alteration and epithelial tumor progression by second harmonic generation microscopy.” *Applied Physics Letters* **96**, 213704 (2010).

29. O Nadiarnykh, RB LaComb, MA Brewer and PJ Campagnola. “Alterations of the extracellular matrix in ovarian cancer studied by S econd Harmonic Generation imaging microscopy.” *BMC Cancer* **10**:94 (2010).

30. HL Fu, B Yu, JY Lo, GM Palmer, TF Kuech, and N Ramanujam. “A low-cost, portable, and quantitative spectral imaging system for application to biological tissues.” *Optics Express*. **18**(12):12630-45 (2010).

31. O Nadiarnykh, S Plotnikov, WA Mohler, I Kalajzic, D Redford-Badwal, PJ Campagnola. "Second harmonic generation imaging microscopy studies of osteogenesis imperfecta." *Journal of Biomedical Optics*. **12**(5):051805 (2007).

32. SB Edge, DR Byrd, and CC Compton. AJCC Cancer Staging Manual (ed 7). Chicago, IL, Springer, (2009).

33. IMAGEJ. WS Rasband, ImageJ, U. S. National Institutes of Health, Bethesda, Maryland, USA, http://imagej.nih.gov/ij/, 1997-2011

34. ES Hwang, S DeVries, KL Chew, DH Moore 2nd, K Kerlikowske, A Thor, BM Ljung, and FM Waldman. "Patterns of chromosomal alterations in breast ductal carcinoma in situ." *Clinical Cancer Research*. **10**(15):5160-7 (2004).

35. N Wasif, MA Maggard, CY Ko and AE Giuliano. "Invasive lobular vs. ductal breast cancer: a s tage-matched comparison of outcomes." *Annals of Surgical Oncology* **17**(7):1862-9 (2010).

36. S Kennedy, J Geradts, T Bydlon, JQ Brown, J Gallagher, M Junker, W Barry, N Ramanujam and L Wilke. "Optical breast cancer margin assessment: an observational study of the effects of tissue heterogeneity on optical contrast." *Breast Cancer Research* **12**(6): R91(2010).

37. IJ Bigio, SG Bown, G Briggs, C Kelley, S Lakhani, D Pickard, PM Ripley, IG Rose and CSaunders. "Diagnosis of breast cancer using elastic-scattering spectroscopy: preliminary clinical results." *Journal of Biomedical Optics* **5**(2): 221-8 (2000).

38. FT Nguyen, AM Zysk, EJ Chaney, JG Kotynek, UJ Oliphant, FJ Bellafiore, KM Rowland, PA Johnson and SA Boppart. "Intraoperative evaluation of breast tumor

margins with optical coherence tomography." *Cancer Research* **69**(22): 8790-6 (2009).

39. AS Haka, Z Volynskaya, JA Gardecki, J Nazemi, R Shenk, N Wang, RR Dasari, M Fitzmaurice, and MS Feld. "Diagnosing breast cancer using Raman spectroscopy: prospective analysis." *Journal of Biomedical Optics* **14**(5): 054023 (2009).
40. X Han and E Brown. "Measurement of the ratio of forward-propagating to back-propagating second harmonic signal using a single objective." *Optics Express* **18**(10):10538-50 (2010).

Figure Legends

Figure 1: Sample images of 5 types of tissue analyzed in this study, from top to bottom: healthy tissue, DCIS, LCIS IDC, and ILC. Left column shows H&E staining, middle shows forward-scattered SHG and right shows F/B ratio

Table 1: Table of the tissue microarray slides that were used, along with how many samples from each slide were used to create each set of results. The number given (i.e. "BR1921") is the part number of the Biomax microarray slide, while "URMC" refers to the full section and tissue microarray (TMA) slide manufactured by the University of Rochester Department of Pathology. Note that samples are "double counted" in that a sample that is IDC T1 and N0 would count in both the IDC T1 column as well as the IDC N0 column.

Figure 2: F/B ratio throughout (a) ductal carcinoma progression and (b) increasing grade in IDC, or decreasing tumor cell differentiation. These results show no difference between DCIS (n=20) and healthy tissue (n=37), but there was a significant difference between IDC (n=147) and the two other tissue types. As the IDC tumor progresses into higher grades the F/B ratio differs significantly from healthy tissue. Specifically, there is no difference between healthy and Grade 1 IDC (n=8), but both of these are significantly higher than Grade 2 IDC (n=88). Grade 3 (n=15) is significantly lower than healthy tissue. Error bars represent standard error.

Figure 3: F/B ratio as a function of (a) T-stage, (b) M-status and (c) N-stage. Healthy tissue (n=37) was significantly higher than all T stages (sample sizes of T1-T4 were n=12, n=97, n=24, and n=11 respectively). (b) The average F/B ratio of M1 tumors (n=9) was not significantly

different than the M0 tumors (n=136). (c) The F/B of healthy tissue was significantly greater than that of N0 (n=51), N1 (n=52) and N2 (n=29), but was not significantly different than N3 (n=9). (d) F/B of N3 tumors, which have 10 or greater lymph node metastatic events, is significantly greater than tumors with less lymph node involvement, i.e. N0-N2 tumors. (e) F/B color map of Healthy Tissue (Top), N0 IDC (middle) and N3 IDC (bottom). Error bars represent standard error and * signifies difference from all other groups being compared.

Figure 4: (a) F/B ratio of ILC (n=153) is not significantly different than IDC (n=145), but are both significantly lower than healthy breast tissue (n=37). F/B ratio of ILC as a function of progression from healthy tissue to *in situ* tissue, to invasive carcinoma (b), N-stage (c) and T-stage (d). LCIS (n=8) and ILC are both significantly lower than healthy breast tissue. Similarly all N-stage ILC tumors are significantly lower than healthy tissue (n=49, n=29, n=11, and n=4, for N0-N3 respectively) . T1 (n=29), T2 (n=96), and T3(n=12) ILC tumors are all had significantly lower F/B ratios than healthy tissue, but T4 (n=10) tumors were not significantly different than healthy. Error bars represent standard error, and * signifies difference from all other groups being compared.

Table 1

	Healthy	DCIS	IDC T				IDC N				IDC M		Grade			LCIS	ILC T				ILC N			
			T1	*T2*	*T3*	*T4*	*N0*	*N1*	*N2*	*N3*	*M1*	*M0*	*1*	*2*	*3*		*T1*	*T2*	*T3*	*T4*	*N0*	*N1*	*N2*	*N3*
1921	30		7	55	7	6	30	34	8			75	4	57	12		5	49	5	4	42	19	4	
20830			5	25	6	5	12	13	13	4		42	4	31	3									
954	7			17	10		9	5	8	5	9	19												
805																1	4	12	1		8	5	5	1
URMC TMA		20																						
URMC Full section																8								3

Figure 1

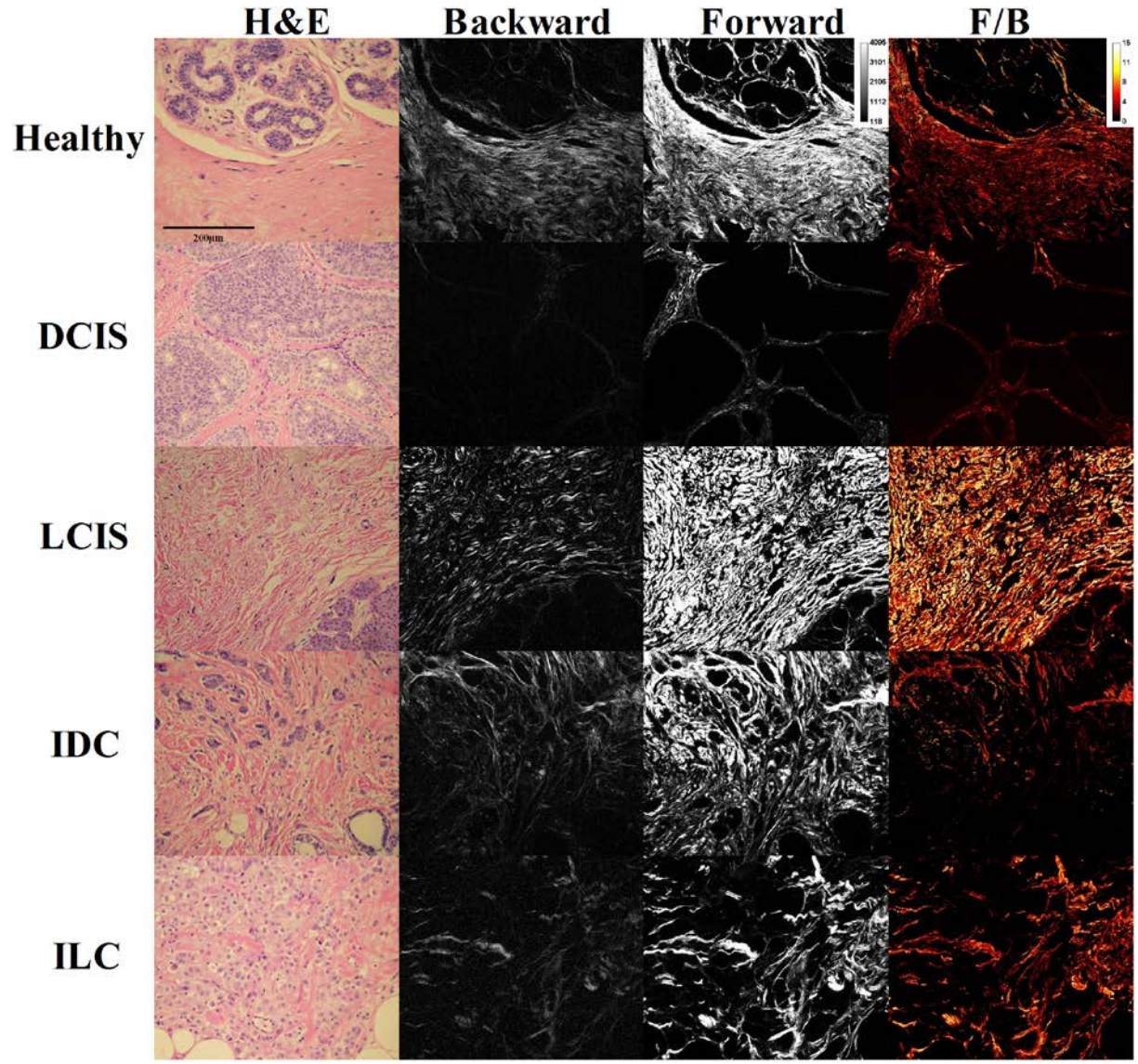

Figure 2

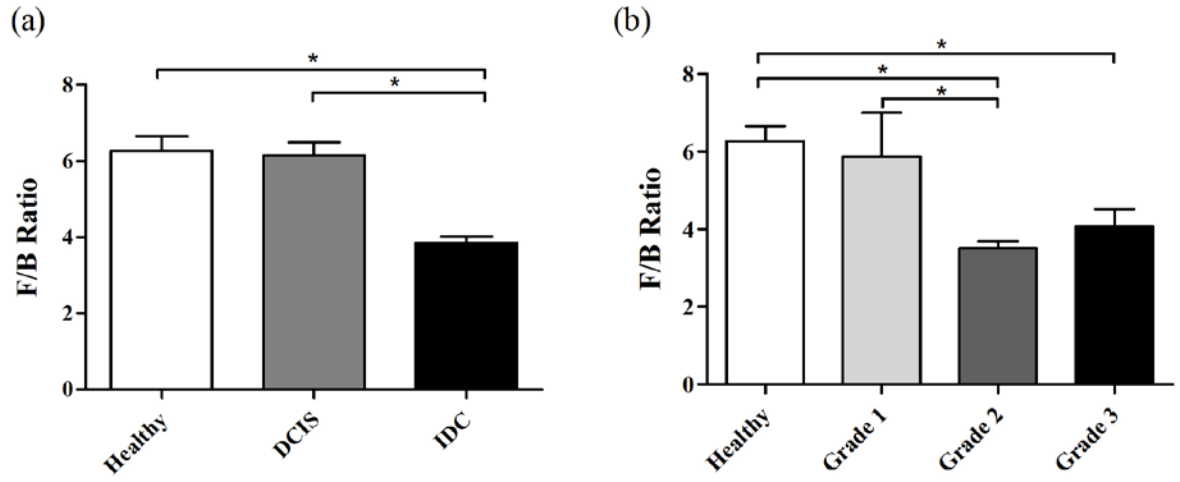

Figure 3

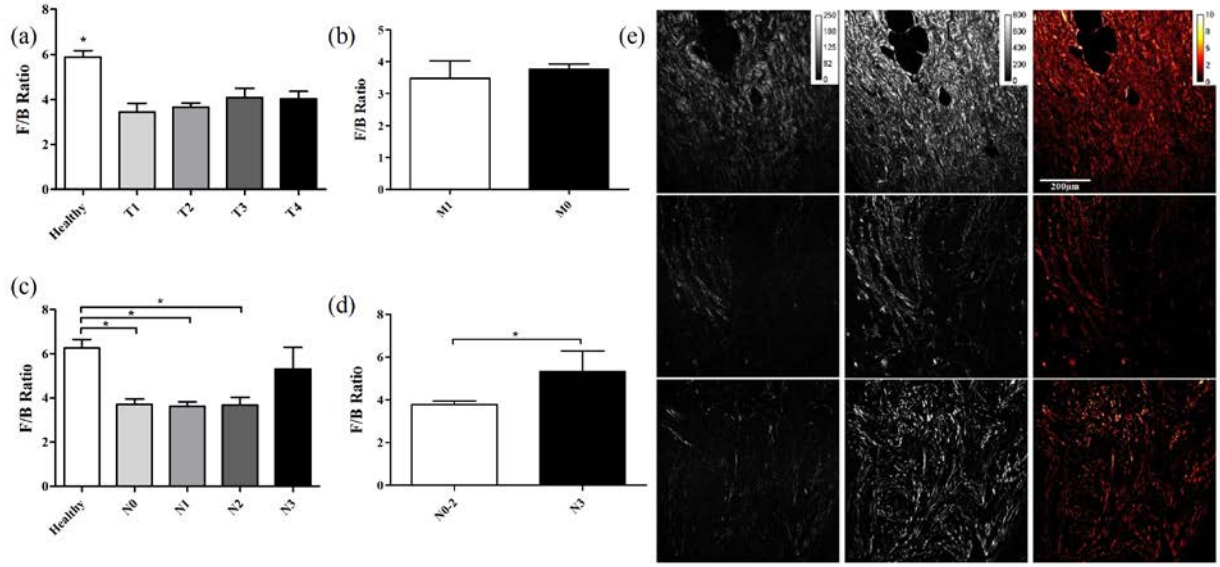

Figure 4

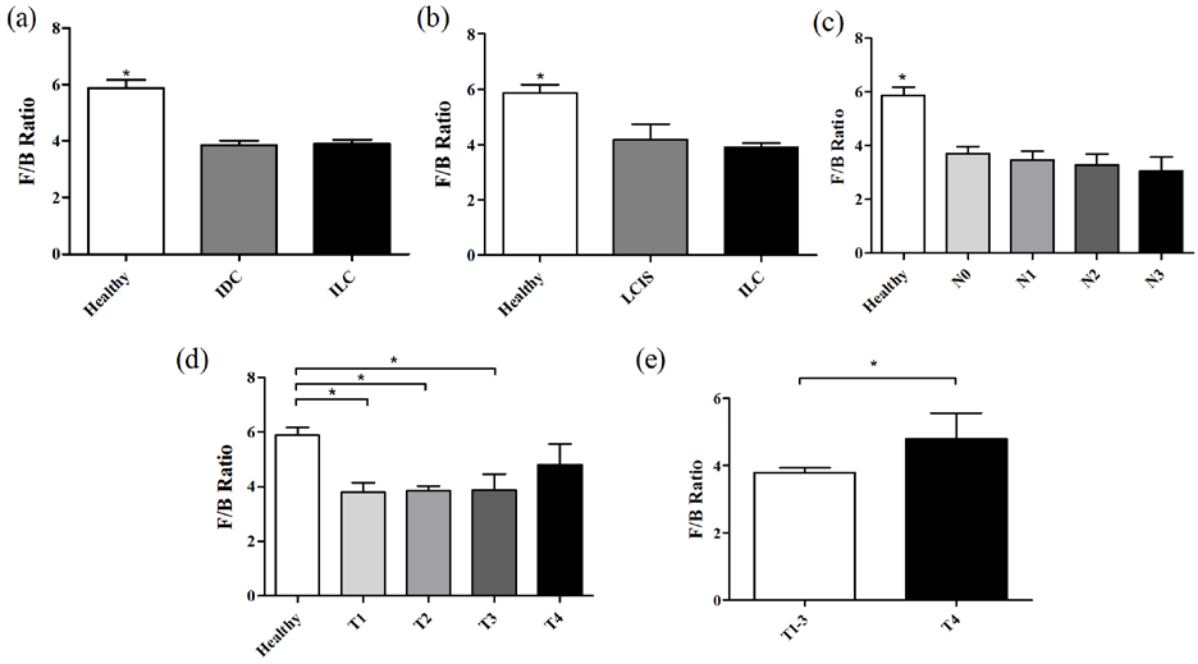
(a)
F/B Ratio
Healthy
IDC
ILC
(b)
F/B Ratio
Healthy
LCIS
ILC
(c)
F/B Ratio
Healthy
N0
N1
N2
N3
(d)
F/B Ratio
Healthy
T1
T2
T3
T4
(e)
F/B Ratio
T1-3
T4

Key Research Accomplishments in the third year:

Used clodronate liposomes to ablate tumor associated macrophages *in vivo*, in the presence and absence of stromal IL-10, and determined that this ablation also affected collagen ordering as well as metastatic output in a manner that indicated stromal TNF-a acting on macrophages was the mechanism whereby OI was altered.

Finished an extensive study of how SHG can be used to reveal matrix structural alterations in human tumor samples on t issue microarrays, and derived several important insights into those alterations, the two most intriguing being 1) that DCIS does not influence adjacent matrix microstructure while LCIS does, and 2) that IDC reveals a significantly lower SHG F/B scattering ration relative to healthy tissue for non-and low-metastatic tumors, but that for the most metastatic tumors (N3) the SHG F/B returns to levels consistent with healthy tissue.

Reportable Outcomes:

Over the past year I published three papers based upon work funded all or in part by this award:

Bouta E, Wood R, Perry S, Brown E, Ritchlin C, Xing L, Schwarz E. (2011) Measuring intranodal pressure and lymph viscosity to elucidate mechanisms of arthritic flare and therapeutic outcomes. Ann N Y Acad Sci. 1240(1):47-52.

Perry S, Burke R, Brown E. (2012) Two Photon and Second Harmonic Microscopy in Clinical and Translational Cancer Research. Invited Review Annals of Biomedical Engineering. 40(2) 277-291.

Madden K, Szpunar M, Brown E. (2012) Early Impact of Social Isolation and Breast Tumor Progression in Mice. Brain Behavior and Immunity. Epub ahead of print.

I have also submitted one manuscript based upon work funded in whole or in part by this grant, and it is attached to this document as part of the main text of the report:

Burke K, Tang P, Brown E. SHG reveals matrix alterations during breast tumor progression.

Conclusion

In conclusion, I believe that I have made significant progress on the goals outlined in my Era of Hope Scholar Research Award.